Determination of Bulk Properties of Tropical Cloud Clusters from Large-Scale Heat and Moisture Budgets

MICHIO YANAI, STEVEN ESBENSEN AND JAN-HWA CHU

Dept. of Meteorology, University of California, Los Angeles 90024

(Manuscript received 29 December 1972)

ABSTRACT

The bulk properties of tropical cloud clusters, such as the vertical mass flux, the excess temperature, and moisture and the liquid water content of the clouds, are determined from a combination of 1) the observed large-scale heat and moisture budgets over an area covering the cloud cluster, and 2) a model of a cumulus ensemble which exchanges mass, heat, water vapor and liquid water with the environment through entrainment and detrainment. The method also provides an understanding of how the environmental air is heated and moistened by the cumulus convection. An estimate of the average cloud cluster properties and the heat and moisture balance of the environment, obtained from 1956 Marshall Islands data, is presented.

1. Introduction

Advances in our understanding of the dynamics of tropical disturbances call for the clarification of a long-standing problem, i.e., the relationship between the large-scale motion and organized cumulus convection.

The important role played by deep cumulus clouds in the heat balance of the tropical atmosphere was first pointed out by Riehl and Malkus (1958). They showed that deep cumulus clouds can carry the released latent heat of condensation to the upper troposphere where the local vertical gradient of moist static energy ($h = c_p T + gz + Lq$) is positive. The role of penetrative cumulus towers in the formation and growth of tropical cyclones was discussed by Riehl and Malkus (1961) and by Yanai (1961a, b). They proposed that cumulus convection, as a heating mechanism, must be adequately parameterized in the framework of the large-scale motion. The first theoretical formulation of the cumulus, macro-motion coupling through boundary layer convergence was made by Charney and Eliassen (1964) and Ooyama (1964, 1969a), in their attempts to explain the growth of tropical cyclones.

In the case of weaker tropical disturbances, such as easterly waves (Riehl, 1945, 1948, 1954; Palmer, 1952), the connection with cumulus convection remained somewhat vague, although the control of cloud organization and precipitation by the large-scale motion had been suggested in a number of studies (e.g., Riehl, 1954; Malkus, 1958; Malkus and Riehl, 1964).

Based on an inspection of cloud pictures taken by satellites during 1967, the JOC Study Group on Tropical Disturbances (1970) documented unquestionable evidence of the organization of maritime tropical clouds into "cloud clusters." The high degree of organization of convective clouds into clusters suggested their likely association with large-scale wave disturbances. Evidence of a systematic westward propagation of the cloud clusters was presented by Chang (1970).

In parallel with the recognition of tropical cloud clusters, rapid progress has been made in observational and theoretical studies of tropical wave disturbances [see review articles of Wallace (1971) and Yanai (1971a)]. We now have several working hypotheses concerning the origin of the waves and their interaction with organized cumulus convection. The so-called "wave, cloud-cluster interaction" has become a leading problem in tropical meteorology.

Recent studies of the energetics of the tropical wave disturbances favor the view that the wave disturbances derive their kinetic energy primarily from the eddy available potential energy which is generated by the release of the latent heat of condensation (Manabe and Smagorinsky, 1967; Manabe et al., 1970; Nitta, 1970, 1972a; Wallace, 1971). The theory of how tropical waves respond to the heating of the condensation has been advanced by Ooyama (1969b), Yamasaki (1969), Hayashi (1970), Holton (1971), T. Murakami (1972), and others. Holton et al. (1971) and Yamasaki (1971) further showed that the waves can be enhanced at certain critical latitudes where the Coriolis parameter equals the frequency of the waves. This is because of the singular response of the boundary layer which controls the large-scale moisture convergence.

To further advance the theory of tropical waves, and to improve the numerical simulation of the tropical general circulation, a much better knowledge of the properties of tropical cloud clusters is needed. Re-

cently, Williams (1970) and Reed and Recker (1971) studied the average macro-structure of the cloud clusters by making composites of many clusters. Reed and Recker (1971) and Nitta (1972a) obtained vertical profiles of the heat source associated with the average cloud cluster.

This study uses a somewhat different approach to obtain the average structure of a cloud cluster and its interaction with the environment. The study was made in parallel with Prof. Akio Arakawa's effort to improve the parameterization of cumulus convection in the UCLA General Circulation Model (Arakawa, 1969, 1971, 1972; Arakawa and Schubert, 1973). It is evident that a large amount of latent heat is liberated in cumulus clouds and the released heat is transported upward, but *how this heat is utilized in warming the large-scale environment* is not so obvious. We must have a better understanding of this physical process to improve cumulus parameterization.[1]

We shall demonstrate that the observed large-scale heat and moisture budgets, together with a simple model of a cumulus ensemble, make it possible to obtain a large amount of information such as the mass flux, the excess temperature, and the moisture and the liquid water content of the cumulus clouds. We shall then show how the observed heat and moisture budgets of the large-scale environment can be explained in terms of induced downward motion between the clouds and the detrainment of water vapor and liquid water from the clouds.

2. Method

a. Preliminary considerations

For convenience, we define the *dry static energy* as

$$s \equiv c_p T + gz, \tag{1}$$

and the *moist static energy* as

$$h \equiv c_p T + gz + Lq, \tag{2}$$

where s is the sum of enthalpy and potential energy and h the sum of s and latent energy. For dry adiabatic processes,

$$\frac{ds}{dt} \approx 0, \tag{3}$$

while for both dry and moist adiabatic processes,

$$\frac{dh}{dt} \approx 0. \tag{4}$$

We consider an ensemble of cumulus clouds which is embedded in a tropical large-scale motion system.

Then we imagine a horizontal area that is large enough to contain the ensemble of clouds, but small enough to be regarded as a fraction of the large-scale system.

We now write the equations of mass continuity, heat energy and moisture continuity, averaged over the hypothesized area:

$$\overline{\nabla \cdot \mathbf{V}} + \frac{\partial \bar{\omega}}{\partial p} = 0, \tag{5}$$

$$\frac{\partial \bar{s}}{\partial t} + \overline{\nabla \cdot s\mathbf{V}} + \frac{\partial \overline{s\omega}}{\partial p} = \overline{Q_R} + L(c - e), \tag{6}$$

$$\frac{\partial \bar{q}}{\partial t} + \overline{\nabla \cdot q\mathbf{V}} + \frac{\partial \overline{q\omega}}{\partial p} = e - c. \tag{7}$$

In the above, most of the notations are conventional; $\bar{\omega}$ is the average vertical p-velocity, Q_R the heating rate due to radiation, c the rate of condensation per unit mass of air, and e the rate of re-evaporation of cloud droplets. The horizontal averages are denoted by $\overline{(\ )}$.

Eqs. (6) and (7) may be rearranged to give

$$Q_1 \equiv \frac{\partial \bar{s}}{\partial t} + \overline{\nabla \cdot s\mathbf{V}} + \frac{\partial \bar{s}\bar{\omega}}{\partial p} = \overline{Q_R} + L(c - e) - \frac{\partial}{\partial p}\overline{s'\omega'}, \tag{8}$$

$$Q_2 \equiv -L\left(\frac{\partial \bar{q}}{\partial t} + \overline{\nabla \cdot q\mathbf{V}} + \frac{\partial \bar{q}\bar{\omega}}{\partial p}\right) = L(c - e) + L\frac{\partial}{\partial p}\overline{q'\omega'}, \tag{9}$$

where deviations from the horizontal averages are denoted by primes. It will be assumed that small-scale eddies in the horizontal components of wind have no significant correlations with s' and q'. But the presence of cumulus convection, and turbulent motion in the sub-cloud layer, may cause significant vertical eddy transports of heat and moisture. Eq. (8) shows that the *apparent heating* Q_1 of the large-scale motion system consists of the heating due to radiation, the release of latent heat by net condensation, and vertical convergence of the vertical eddy transport of sensible heat. Eq. (9) is the equation of moisture continuity expressed in units of heating rate, with Q_2 being a measure of the *apparent moisture sink* which is due to the net condensation and vertical divergence of the vertical eddy transport of moisture.

From (8) and (9), we obtain

$$Q_1 - Q_2 - \overline{Q_R} = -\frac{\partial}{\partial p}\overline{(s' + Lq')\omega'} = -\frac{\partial}{\partial p}\overline{h'\omega'}, \tag{10}$$

where $\overline{h'\omega'}$ is a measure of the vertical eddy transport of total heat and may be used to measure the activity of cumulus convection. For later convenience we define

---

[1] Earlier attempts of parameterization of cumulus convection were reviewed by Yanai (1971a), Bates (1972) and Ogura (1973).

the vertical eddy flux of total heat by

$$F \equiv -\frac{1}{g}\overline{h'\omega'} = \frac{1}{g}\int_{p_T}^{p}(Q_1-Q_2-Q_R)dp, \qquad (11)$$

where p_T is the pressure at the cloud top.

Integrating (8) from p_T to p_0 (the pressure at the sea surface),

$$\frac{1}{g}\int_{p_T}^{p_0}(Q_1-Q_R)dp = \frac{L}{g}\int_{p_T}^{p_0}(c-e)dp-\frac{1}{g}\overline{(s'\omega')}_{p=p_0}$$

$$\approx LP_0+\rho_0 c_p\overline{(T'w')}_{p=p_0}$$

$$= LP_0+S_0, \qquad (12)$$

where P_0 and S_0 are, respectively, the amount of precipitation and the supply of sensible heat from the ocean surface.

Integrating (9) from p_T to p_0,

$$\frac{1}{g}\int_{p_T}^{p_0}Q_2 dp = \frac{L}{g}\int_{p_T}^{p_0}(c-e)dp+\frac{L}{g}\overline{(q'\omega')}_{p=p_0}$$

$$\approx LP_0-\rho_0 L\overline{(q'w')}_{p=p_0}$$

$$= L(P_0-E_0), \qquad (13)$$

where E_0 is the rate of evaporation from the sea.

From (11), (12) and (13), we find

$$F_0 \equiv F(p_0) = S_0+LE_0. \qquad (14)$$

Eqs. (12)–(14) can be used to check the accuracy of the estimates of Q_1, Q_2 and Q_R against surface observations of P_0, S_0 and E_0.

b. Cloud mass flux

The large-scale vertical motion $\bar{\omega}$ is the average of the mean ascent in active cumulus clouds and the slow descent or ascent of the environmental air. For simplicity we define the average mass flux across a unit horizontal area by[2]

$$\bar{M} \equiv -\bar{\omega}, \qquad (15)$$

and divide $\bar{M}$ into two parts,

$$\bar{M} = M_c+\tilde{M}, \qquad (16)$$

M_c being the upward mass flux in the active cumulus clouds, and $\tilde{M}$ the residual mass flux in the environment. We assume that the active clouds occupy a fraction σ of the horizontal area. Then

$$\left.\begin{array}{l} M_c = -\sigma\omega_c \\ \tilde{M} = -(1-\sigma)\tilde{\omega} \end{array}\right\}, \qquad (17)$$

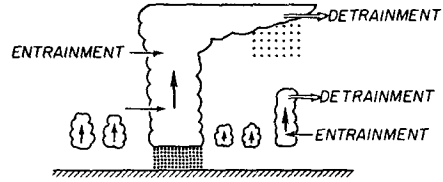[2] Dimensionally, it may be more logical to define the mass flux by $M \equiv -\omega/g \approx \rho w$.

FIG. 1. Schematic view of an ensemble of cumulus clouds.

where ω_c is a typical vertical p-velocity in the clouds and $\tilde{\omega}$ a typical vertical velocity in the environment; $\tilde{\omega}$ may be quite different from $\bar{\omega}$. For example, if all the ascent required by the large-scale convergence takes place in the cumulus clouds, $\bar{\omega}=\sigma\omega_c$ and $\tilde{\omega}=0$. If all the ascent is compensated by the descent between clouds, $\bar{\omega}=0$ and $(1-\sigma)\tilde{\omega}=-\sigma\omega_c$.

We next assume that the dry static energy s and mixing ratio q have characteristic values inside the active clouds, which are denoted by s_c and q_c, respectively. The characteristic values of s and q in the environment are denoted by $\tilde{s}$ and $\tilde{q}$. Therefore,

$$\left.\begin{array}{l} \bar{s}=\sigma s_c+(1-\sigma)\tilde{s} \\ \bar{q}=\sigma q_c+(1-\sigma)\tilde{q} \end{array}\right\}. \qquad (18)$$

It is important to note that

$$\left.\begin{array}{l} \bar{s}=\sigma(s_c-\tilde{s})+\tilde{s}\approx\tilde{s} \\ \bar{q}=\sigma(q_c-\tilde{q})+\tilde{q}\approx\tilde{q} \end{array}\right\}, \qquad (19)$$

because

$$\sigma\ll 1, \quad (s_c-\tilde{s})<\tilde{s} \quad \text{and} \quad (q_c-\tilde{q})\lesssim\tilde{q}.$$

Let us assume that above the cloud base the vertical eddy transports of s and q are solely due to the presence of active cumulus convection. Then,

$$\left.\begin{array}{l} \overline{s'\omega'}=\overline{s\omega}-\bar{s}\bar{\omega}=\sigma(1-\sigma)(s_c-\tilde{s})(\omega_c-\bar{\omega}) \\ \overline{q'\omega'}=\overline{q\omega}-\bar{q}\bar{\omega}=\sigma(1-\sigma)(q_c-\tilde{q})(\omega_c-\bar{\omega}) \end{array}\right\}. \qquad (20)$$

Because of the foregoing reasons, we readily obtain

$$-\overline{s'\omega'}\approx-\sigma\omega_c(s_c-\tilde{s})=M_c(s_c-\tilde{s}), \qquad (21a)$$

$$-\overline{q'\omega'}\approx-\sigma\omega_c(q_c-\tilde{q})=M_c(q_c-\tilde{q}). \qquad (21b)$$

Eq. (21a) shows that the vertical eddy heat flux is given by the product of the cloud mass flux and the temperature excess of the clouds, since $s_c-\tilde{s}=c_p(T_c-\tilde{T})$; Eq. (21b) has a similar interpretation. Such formulations were discussed by Riehl and Malkus (1961) and Yanai (1964). Combining (21a) with (21b), we have also

$$-\overline{h'\omega'}=gF=M_c(h_c-\tilde{h}). \qquad (22)$$

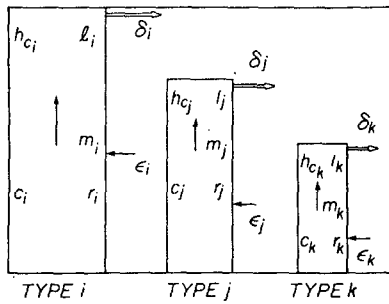Note that F is an observable quantity, as given by (11).

FIG. 2. Idealized view of cumulus cloud types, classified according to their top heights (see text for notation).

The above derivations are correct only when all clouds at a given height share the same values of ω_c, s_c and q_c. In a more realistic situation, we may have a *variety of clouds with different characteristics*. We then generalize (21) and (22) (assuming $\sum_i \sigma_i \ll 1$) by

$$-\overline{s'\omega'} = \sum_i m_i(s_{ci}-\tilde{s}) \atop -\overline{q'\omega'} = \sum_i m_i(q_{ci}-\tilde{q}) \bigg\}, \qquad (23)$$

$$-\overline{h'\omega'} = \sum_i m_i(h_{ci}-\tilde{h}), \qquad (24)$$

where i refers to the ith cloud. We note that

$$M_c = \sum_i m_i. \qquad (25)$$

Thus, we now have

$$Q_1 - Q_R = L\sum_i (c_i-e_i) + \frac{\partial}{\partial p}\sum_i m_i(s_{ci}-\tilde{s}), \qquad (26a)$$

$$Q_2 = L\sum_i (c_i-e_i) - L\frac{\partial}{\partial p}\sum_i m_i(q_{ci}-\tilde{q}), \qquad (26b)$$

where c_i and e_i are the rate of condensation taking place in the ith cloud per unit pressure interval and the rate of re-evaporation of that cloud, respectively.

c. A model of the cumulus ensemble

Consider an ensemble of cumulus clouds as shown in Fig. 1. These clouds are embedded in a large-scale motion system. We shall assume that *the activity of the cumulus clouds is statistically in an equilibrium with the imposed large-scale motion*. Obviously, individual cumulus clouds will undergo their own life cycles. However, we hypothesize that, over a time scale describing the behavior of the large-scale motion system, the cloud ensemble maintains the heat and moisture balance with the environment.

To simplify the treatment, we classify the cumulus clouds according to the heights of the cloud tops.[3]

---

[3] This is equivalent to classifying the clouds according to their radii, because of the well-known entrainment-radius relationship.

We assume that all the clouds have a common cloud base height, and that the values of s_c and q_c (and thus h_c), at a given height, are the same for every cloud which has the same top height. We may then use the suffix i as the index of a classified cloud type, instead of as the index of an individual cloud. The idealization thus introduced is shown in Fig. 2.

The equations of balance for mass, heat, water vapor and liquid water between cloud type i and its environment are written

$$\epsilon_i - \delta_i + \frac{\partial m_i}{\partial p} = 0 \quad \text{(mass)} \qquad (27)$$

$$\epsilon_i \tilde{s} - \delta_i s_{ci} + \frac{\partial m_i s_{ci}}{\partial p} + Lc_i = 0 \quad \text{(heat)} \qquad (28)$$

$$\epsilon_i \tilde{q} - \delta_i q_{ci} + \frac{\partial m_i q_{ci}}{\partial p} - c_i = 0 \quad \text{(water vapor)} \qquad (29)$$

$$-\delta_i l_i + \frac{\partial m_i l_i}{\partial p} + c_i - r_i = 0 \quad \text{(liquid water)} \qquad (30)$$

where ϵ_i and δ_i are the rates of *mass entrainment* and *detrainment* per unit pressure interval. Because of the definition of the cloud mass flux, ϵ_i and δ_i have dimension of the inverse of time; c_i is the rate of condensation, per unit pressure interval, occurring in cloud type i, l_i the mixing ratio of liquid water, and r_i the rate of generation of raindrops which is assumed to fall out immediately. In addition, we assume that the rate of re-evaporation e_i is equal to that of the detrainment of liquid water,[4]

$$e_i = \delta_i l_i. \qquad (31)$$

The above set of equations was presented by Arakawa (1971) and Yanai (1971b). Ooyama (1971) also presented similar equations.

It is convenient to define the *saturation moist static energy* of the environment as

$$\tilde{h}^* \equiv c_p\tilde{T} + gz + L\tilde{q}^*(p,\tilde{T}), \qquad (32)$$

where $\tilde{q}^*$ is the saturation mixing ratio at temperature $\tilde{T}$. Then it follows that

$$s_{ci} - \tilde{s} = \frac{1}{1+\gamma}(h_{ci}-\tilde{h}^*), \qquad (33)$$

$$L(q_{ci}-\tilde{q}^*) = \frac{\gamma}{1+\gamma}(h_{ci}-\tilde{h}^*), \qquad (34)$$

where $\gamma \equiv (L/c_p)(\partial q^*/\partial T)_p$ [after Arakawa (1969)].

We now have the unknowns m_i, δ_i, ϵ_i; s_{ci}, q_{ci}, h_{ci}; c_i, r_i, l_i, e_i. When i_{max} types of cumulus clouds are considered, we have $(7 \times i_{max}+2)$ equations [(27)–(31),

---

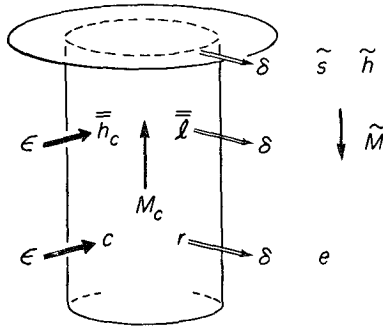[4] Thus, the evaporation of falling raindrops is ignored.

FIG. 3. The idealized model of a cumulus cloud ensemble (see text for notation).

(33), (34) plus (26a, b)]. Obviously these are not sufficient to determine $10 \times i_{max}$ unknowns.

In order to make the problem tractable, we introduce further simplifications. First we note that

$$M_c = \sum_i m_i, \quad \epsilon = \sum_i \epsilon_i, \quad \delta = \sum_i \delta_i, \qquad (35)$$

$$c = \sum_i c_i, \quad r = \sum_i r_i, \quad e = \sum_i e_i. \qquad (36)$$

Then we define a weighted average of h_{ci} by

$$\bar{h}_c = \sum_i m_i h_{ci} / \sum_i m_i = \sum_i m_i h_{ci} / M_c, \qquad (37)$$

and define $\bar{s}_c$, $\bar{q}_c$ and $\bar{l}$ similarly.

We now introduce the following assumptions:

(i) Each type of cloud has a *thin layer of detrainment*, where

$$h_{ci} = \bar{h}^*. \qquad (38)$$

This means that the clouds detrain at the level where they lose buoyancy. When (38) is inserted into (33), the criterion becomes $s_{ci} = \bar{s}$, i.e., $T_{ci} = \bar{T}$. It is also evident from (34) that $q_{ci} = \bar{q}^*$. This assumption is also used by Arakawa (1971) and Arakawa and Schubert (1973). Near the tropopause we need a special consideration because the cloud mass flux entering from below may detrain in this layer regardless of the non-buoyancy condition (38). In this layer the entrainment is assumed to be zero, so that $\delta = \partial M_c / \partial p$. This assumption allows the detrainment of heat as well as moisture to take place near the tropopause.

(ii) The liquid water content of the detrained air, l_i, is the same as $\bar{l}$, i.e.,

$$l_i = \bar{l}. \qquad (39)$$

This gross assumption is needed to close the set of equations.

(iii) The conversion of cloud droplets into raindrops is proportional to the average liquid water content. The rate of precipitation is parameterized by

$$r = K(p)\bar{l}, \qquad (40)$$

where $K(p)$ is an empirical function which varies with height. Because our model of clouds does not explicitly contain the vertical velocity in the clouds, it is not possible to include detailed cloud physical processes.

With these assumptions, we obtain a closed set of equations for the ten unknowns; M_c, ϵ, δ; $\bar{h}_c$, $\bar{s}_c$, $\bar{q}_c$, $\bar{l}$; c, r, e. The equations are as follows:

$$Q_1 - Q_R = L(c-e) + \frac{\partial}{\partial p}[M_c(\bar{s}_c - \bar{s})] \qquad (41)$$

$$Q_2 = L(c-e) - L\frac{\partial}{\partial p}[M_c(\bar{q}_c - \bar{q})] \qquad (42)$$

$$\epsilon - \delta + \frac{\partial M_c}{\partial p} = 0 \qquad (43)$$

$$(\epsilon - \delta)\bar{s} + \frac{\partial M_c \bar{s}_c}{\partial p} + Lc = 0 \qquad (44)$$

$$\epsilon \bar{q} - \delta \bar{q}^* + \frac{\partial M_c \bar{q}_c}{\partial p} - c = 0 \qquad (45)$$

$$-\delta \bar{l} + \frac{\partial M_c \bar{l}}{\partial p} + c - r = 0 \qquad (46)$$

$$= K(p)\bar{l} \qquad (47)$$

$$e = \delta \bar{l}. \qquad (48)$$

In addition, saturation relations, similar to (33) and (34), relate $\bar{s}_c$, $\bar{q}_c$ and $\bar{h}_c$.

In the above, only the terms $Q_1 - Q_R$, Q_2, $\bar{s}$ and $\bar{q}$ are directly observable by means of synoptic-scale soundings.

The simplified model of the cloud ensemble is schematically illustrated in Fig. 3. The ensemble exchanges its mass, heat, moisture and liquid water with its environment. Both entrainment and detrainment can take place at the same height.

Using (43), (44) and (45), we further modify (41) and (42) to obtain

$$Q_1 - Q_R = -M_c \frac{\partial \bar{s}}{\partial p} - Le, \qquad (49)$$

$$Q_2 = LM_c \frac{\partial \bar{q}}{\partial p} - L\delta(\bar{q}^* - \bar{q}) - Le. \qquad (50)$$

These equations were derived by Arakawa (1971), Ooyama (1971) and Yanai (1971b).

Eq. (49) shows that the *apparent heat source*, in addition to Q_R, consists of *an adiabatic warming due to*

a component of downward motion which compensates M_c, and a *cooling due to the re-evaporation of cloud droplets.* Eq. (50) shows that *the apparent moisture sink* is due to a *drying effect by the compensating downward motion* and that *the detrainment of water vapor and the re-evaporation of detrained liquid water act as moisture sources for the environment.* These effects were also discussed by Gray (1971, 1972).

Eliminating e between (49) and (50), we obtain

$$Q_1 - Q_2 - Q_R = \delta(\tilde{h}^* - \tilde{h}) - M_c \frac{\partial \tilde{h}}{\partial p}. \tag{51}$$

Elimination of c between (44) and (45) gives

$$\delta(\tilde{h}^* - \tilde{h}) - M_c \frac{\partial \bar{\tilde{h}}_c}{\partial p} - (\bar{\tilde{h}}_c - \tilde{h}) \frac{\partial M_c}{\partial p} = 0, \tag{52}$$

or

$$\epsilon(\tilde{h}^* - \tilde{h}) = M_c \frac{\partial \bar{\tilde{h}}_c}{\partial p} + \frac{\partial M_c}{\partial p}(\bar{\tilde{h}}_c - \tilde{h}^*). \tag{52a}$$

Because of the presence of the second term on the right of (52a), entrainment does not necessarily give $\partial \bar{\tilde{h}}_c / \partial p > 0$, as in the case of entrainment models of a single cloud (e.g., Levin, 1959; Simpson and Wiggert, 1969; Weinstein, 1970; Warner, 1970; Simpson, 1971; and many others).

Combining (51) with (52), we confirm that

$$Q_1 - Q_2 - Q_R = M_c \frac{\partial}{\partial p}(\bar{\tilde{h}}_c - \tilde{h}) + (\bar{\tilde{h}}_c - \tilde{h}) \frac{\partial M_c}{\partial p}$$

$$= \frac{\partial}{\partial p}[M_c(\bar{\tilde{h}}_c - \tilde{h})]. \tag{53}$$

Vertical integration of (53) gives, using (11),

$$gF = M_c(\bar{\tilde{h}}_c - \tilde{h}). \tag{54}$$

We see that (54) is identical with (22), when only one type of clouds is considered.

d. The conditions at the cloud base

The foregoing set of equations does not apply in the sub-cloud layer. At the cloud base M_c and h_c are determined by the following considerations.

In the sub-cloud layer between p_B and p_0 (see Fig. 4), the heat and moisture budgets are

$$\frac{\Delta p}{g}(Q_1 - Q_R) = S_0 - \frac{M_{cB}}{g} c_p (T_c - \tilde{T})_B, \tag{55}$$

$$\frac{\Delta p}{g} Q_2 = -\frac{L}{g} M_{cB}(q_c - \tilde{q})_B - LE_0, \tag{56}$$

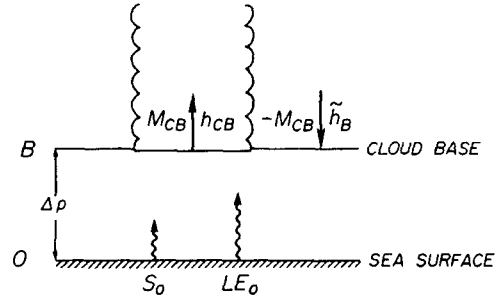where subscript B refers to the cloud base, and

FIG. 4. Energy transfer processes between cloud base and sea surface.

$\Delta p = p_0 - p_B$. Subtracting (56) from (55), we have

$$\frac{\Delta p}{g}(Q_1 - Q_2 - Q_R) = F_0 - \frac{M_{cB}}{g}(h_c - \tilde{h})_B. \tag{57}$$

Using observed values of Q_1, Q_2, Q_R in the sub-cloud layer, and F_0, (57) gives

$$M_{cB}(h_c - \tilde{h})_B = gF_0 - \Delta p(Q_1 - Q_2 - Q_R)$$
$$= gF_B = f_1. \tag{58}$$

Similarly, (55) gives

$$M_{cB} c_p (T_c - \tilde{T})_B = gS_0 - \Delta p(Q_1 - Q_R)$$
$$= f_2. \tag{59}$$

If the Bowen ratio B is known, $S_0 = BF_0 / (1+B)$ so that f_1 and f_2 are known. Because

$$f_1 = M_{cB}(h_c - \tilde{h}^* + \tilde{h}^* - \tilde{h})_B$$
$$= M_{cB}(1+\gamma)c_p(T_c - \tilde{T})_B + M_{cB}(\tilde{h}^* - \tilde{h})_B$$
$$= (1+\gamma)f_2 + M_{cB}(\tilde{h}^* - \tilde{h})_B,$$

where

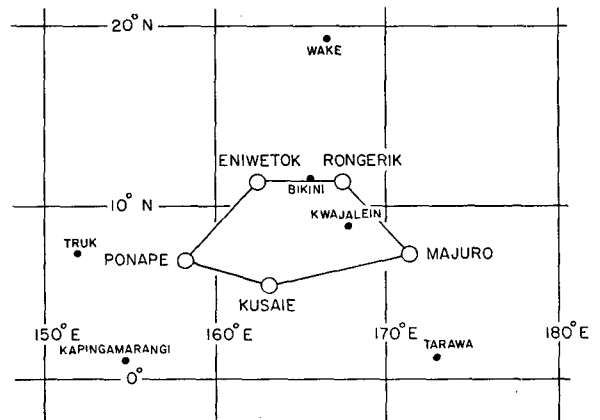$$\gamma \equiv \frac{L}{c_p}\left(\frac{\partial q^*}{\partial T}\right)_p,$$

FIG. 5. Island stations in the Marshall Islands region. The pentagon connecting the five stations indicated by large circles was used for the large-scale budget computations.

we obtain

$$M_{cB} = \frac{f_1 - (1+\gamma)f_2}{\tilde{h}^* - \tilde{h}}, \qquad (60)$$

and

$$h_{cB} - \tilde{h} = f_1 / M_{cB}. \qquad (61)$$

e. Numerical method of solution

After specifying the cloud base conditions, the following set of equations is solved for each cloud layer by iteration:

$$-M_c^{(\nu)} \frac{\partial \tilde{s}}{\partial p} = Q_1 - Q_R + Le^{(\nu-1)} \qquad (62)$$

$$[\tilde{h}_c^{(\nu)} - \tilde{h}] = gF/M_c^{(\nu)} \qquad (63)$$

$$\tilde{s}_c^{(\nu)} - \tilde{s} = \frac{1}{1+\gamma} [\tilde{h}_c^{(\nu)} - \tilde{h}^*] \qquad (64)$$

$$L[\tilde{q}_c^{(\nu)} - \tilde{q}^*] = \frac{\gamma}{1+\gamma} [\tilde{h}_c^{(\nu)} - \tilde{h}^*] \qquad (65)$$

$$\delta^{(\nu)}(\tilde{h}^* - \tilde{h}) = Q_1 - Q_2 - Q_R + M_c^{(\nu)} \frac{\partial \tilde{h}}{\partial p} \qquad (66)$$

$$\epsilon^{(\nu)} = \delta^{(\nu)} - \frac{\partial M_c^{(\nu)}}{\partial p} \qquad (67)$$

$$c^{(\nu)} = \frac{\partial}{\partial p} [M_c^{(\nu)=(\nu)} \tilde{q}_c] - \frac{\partial M_c^{(\nu)}}{\partial p} \tilde{q} - \delta^{(\nu)}(\tilde{q}^* - \tilde{q}) \qquad (68)$$

$$[\delta^{(\nu)} + K] \tilde{l}^{(\nu)} - \frac{\partial M_c^{(\nu)} \tilde{l}^{(\nu)}}{\partial p} = c^{(\nu)} \qquad (69)$$

$$r^{(\nu)} = K \tilde{l}^{(\nu)} \qquad (70)$$

$$e^{(\nu)} = \delta^{(\nu)} \tilde{l}^{(\nu)}. \qquad (71)$$

In the above, ν is the index of iteration.

We start with (62), taking an initial guess $e^{(0)} = 0$. Among the above ten equations, only the liquid water equation (69) is a differential equation. We note that, at the final converged step, M_c, δ, ϵ, c, $\tilde{l}$ must be non-negative.

3. Data

To test the computational scheme outlined in Section 2, daily vertical profiles of Q_1, Q_2 and Q_R, which are representative over an area, say a 300-km square, are needed. Ideally, these must be supplemented by daily values of precipitation and heat and moisture transfer

from the ocean surface. To the authors' knowledge, such an ideal data set does not exist.

We selected the set of upper air, surface and ship observations of Operation Redwing, which was collected in the Marshall Islands area during the period from 15 April to 22 July, 1956 (Joint Task Force Seven, 1956). This special data set was used in the studies of Rosenthal (1960), Nitta (1970, 1972a, b), M. Murakami (1971, 1972), Janota (1971) and Hastenrath (1972) for various purposes. During the period of observation, a number of disturbances passed through the area.

For practical geometrical considerations, we selected five stations which form a pentagonal region whose area is $\sim 62 \times 10^4$ km² (Fig. 5). In addition, surface observations taken aboard the U.S.S. *Estes*, stationed near Bikini Island, were also used. At the five stations, all the upper air soundings were made four times a day (0300, 0900, 1500, 2100 GMT), while all the surface and the ship observations were made four or eight times a day, depending on the meteorological elements. To insure the accuracy of lateral flux computations, all the standard and the significant level radio soundings and the wind aloft data were combined and re-edited at UCLA. The processed data are layer-averaged winds, temperature and moisture at intervals of 50 mb. These were used to obtain the estimates of Q_1 and Q_2.

4. Large-scale mass, heat and moisture budgets

a. Procedure

The method for obtaining the large-scale vertical motion $\bar{\omega}$, the apparent heat source Q_1, and the apparent moisture sink Q_2 is basically similar to those used by Yanai (1961a, 1963), Nitta (1970, 1972a) and Reed and Recker (1971), but a somewhat refined computational scheme for the horizontal integrations was used in this study (see Appendix).

The area-averaged horizontal divergence and relative vorticity over the pentagonal region were computed by

$$\overline{\nabla \cdot \mathbf{V}} = \frac{1}{A} \left(\oint u \, dy - \oint v \, dx \right), \qquad (72)$$

$$\bar{\zeta} = \frac{1}{A} \left(\oint u \, dx + \oint v \, dy \right), \qquad (73)$$

where u and v are the eastward and the northward components of the winds along the periphery of the pentagon whose area is denoted by A.

The average vertical p-velocity is obtained by

$$\bar{\omega} = \int_{p_0}^{p} \overline{\nabla \cdot \mathbf{V}} \, dp. \qquad (74)$$

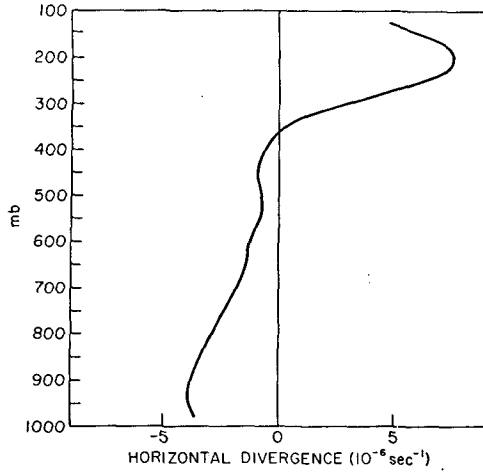The original estimates of $\overline{\nabla \cdot \mathbf{V}}$ were slightly corrected to
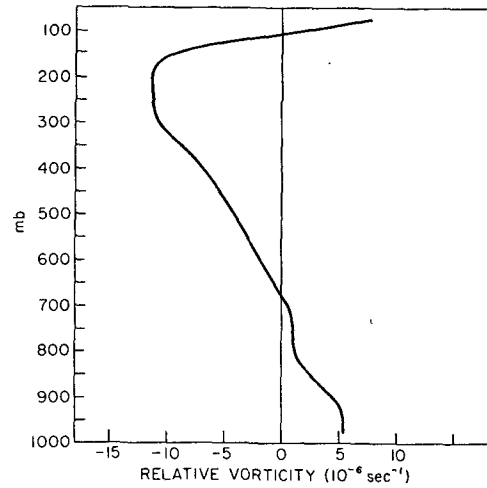
FIG. 6. The mean horizontal divergence.

make $\bar{\omega}$ vanish at 100 mb. A linear correction of $\overline{\nabla \cdot \mathbf{V}}$, increasing with height, was used.
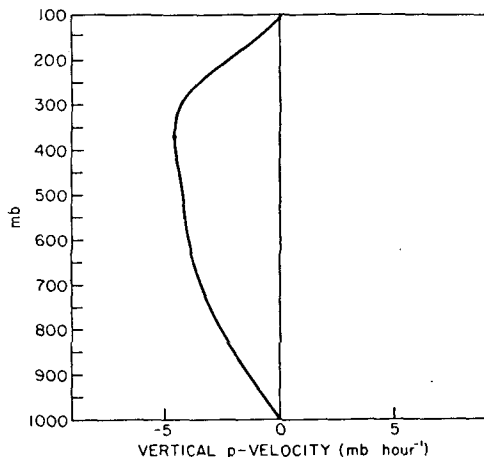
The rate of heating due to the apparent heat source Q_1 was computed by the first law of the thermodynamics,

$$\frac{Q_1}{c_p} = \frac{\partial \bar{T}}{\partial t} + \overline{\mathbf{V} \cdot \nabla T} + \bar{\omega}\left(\frac{\partial \bar{T}}{\partial p} - \frac{\bar{\alpha}}{c_p}\right)$$

$$= \frac{\partial \bar{T}}{\partial t} + (\overline{\nabla \cdot T\mathbf{V}} - \overline{T\nabla \cdot \mathbf{V}}) + \frac{\bar{\omega}}{c_p}\frac{\partial \bar{s}}{\partial p}. \qquad (75)$$

The rate of equivalent heating due to the apparent moisture sink Q_2 was obtained by

$$\frac{Q_2}{c_p} = -\frac{L}{c_p}\left(\frac{\partial \bar{q}}{\partial t} + \overline{\nabla \cdot q\mathbf{V}} + \frac{\partial \bar{q}\bar{\omega}}{\partial p}\right). \qquad (76)$$

The corrections on $\overline{\nabla \cdot \mathbf{V}}$ and $\bar{\omega}$ were introduced into (75) and (76) so as not to violate (74).

FIG. 7. The mean vertical p-velocity.

FIG. 8. The mean relative vorticity.

Because of the lack of humidity soundings above the 250-mb level, a constant relative humidity (50%) was assumed between the 100- and 250-mb levels, although some earlier studies (Mastenbrook, 1965, 1968) suggest higher humidity values in the tropical upper troposphere.

All the computations were carried out at every observation time (390 samples) and at intervals of 50 mb. In this section we mention only the time averages of all the samples. An investigation of the variation in time of the large-scale parameters will be reported in another paper.

b. Divergence, vertical velocity and vorticity

The vertical profile of the average horizontal divergence is shown in Fig. 6. There is a deep layer of convergence up to the 350-mb level and a shallow layer of intense divergence aloft. These features are similar to the results obtained by Williams (1970) and Reed and Recker (1971) for active cloud clusters. On the average, there is no evidence of concentrated mass convergence in the boundary layer.

The average vertical profile of the mean vertical p-velocity is shown in Fig. 7. The upward velocity reaches its maximum at the 350-mb level.

As a by-product, vertical profiles of relative vorticity were also obtained. The time averaged profile is shown in Fig. 8. The vorticity is positive in the lower troposphere and strongly negative in the upper troposphere. These features are similar to those computed by Yanai (1963) using the 1958 test data. The profile is also very similar to those obtained by Williams (1970) and Reed and Recker (1971) for active cloud clusters.

c. Static energy

Mean vertical profiles of the dry static energy $\bar{s}$, the moist static energy $\bar{h}$, and its saturation value $\bar{h}^*$ are
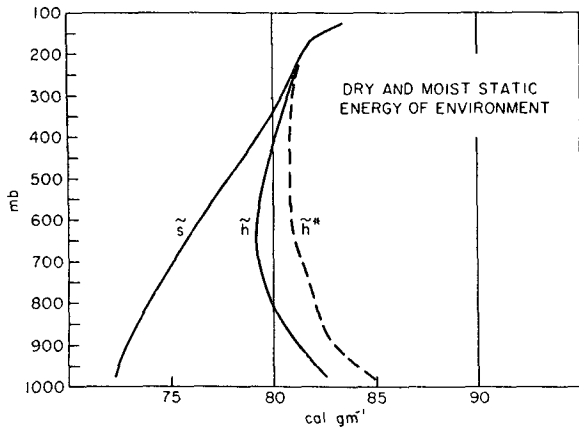
FIG. 9. The mean dry static energy $\tilde{s}$, moist static energy $\tilde{h}$ (both solid), and saturation moist static energy $\tilde{h}^*$ (dashed) of the environment.
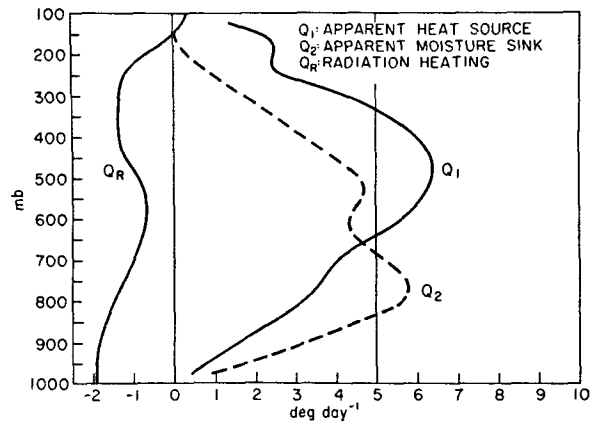

FIG. 10. The mean apparent heat source Q_1 (solid) and moisture sink Q_2 (dashed). On the left is the radiational heating rate given by Dopplick (1970).

shown in Fig. 9. All the values below the 450-mb level are systematically higher than the corresponding values obtained by Riehl and Malkus (1958) for the mean equatorial trough zone, and by Hastenrath (1971) for Palmyra and Christmas Island.

In the lower troposphere $\tilde{h}$ is much larger than $\tilde{s}$, owing to the presence of moisture; $\tilde{h}$ has a minimum at 625 mb. In the upper troposphere $\tilde{h}$ approaches $\tilde{s}$ and the distinction between the two curves becomes negligible above the 200-mb level. The existence of such a minimum of $\tilde{h}$, with the upward increase of $\tilde{h}$ in the upper troposphere, led Riehl and Malkus (1958) to hypothesize a process of selective upward transport of heat by "hot towers."

Note also that values of $\tilde{h}$ in the lower and middle troposphere are much below the saturation values $\tilde{h}^*$ which show a marked constancy in the layer between 300 and 600 mb. In contrast to the other large-scale parameters, the day-to-day variations of $\tilde{s}$ and $\tilde{h}$ are small regardless of the passage of disturbances. This fact suggests that cumulus convection occurs in response to the large-scale forcing in such a way that the observed profile of $\tilde{h}$ is maintained.

d. Apparent heat source and apparent moisture sink

The time-averaged vertical profiles of Q_1 and Q_2 are shown in Fig. 10. Both are expressed in units of heating rate (°C day^{-1}). Note that there is a considerable difference between them. This was already noted in a study of typhoon formation (Yanai, 1961a) and was used by Wada (1969) and Nitta (1972a) to measure the activity of cumulus convection. The averaged Q_1 has a maximum (6.4C day^{-1}) at 475 mb. On the other hand, the average Q_2 has its principal maximum at a much lower level (775 mb) and a secondary peak at 525 mb. The profile of Q_1 is very similar to those obtained by Reed and Recker (1971) and Nitta (1972a).

With the daily vertical profiles of Q_1 and Q_2, we can

obtain the required vertical flux of eddy heat transport, $F = -\overline{(h'\omega')}/g$, provided that the daily vertical profiles of the radiative heating rate Q_R are known.

Unfortunately, we have no direct measurements of Q_R in conjunction with the upper air soundings. In this experimental study, we use the climatological vertical profile of Q_R given by Dopplick (1970). The profile averaged from his Figs. 26 and 27 (between the equator and 10N) is shown on the left side of Fig. 10. The net radiational cooling in the troposphere is on the order of 1–2C day^{-1}. This profile is very similar to the profiles of infrared cooling alone, as measured in the tropics with the Suomi-Kuhn infrared radiometer (Riehl, 1962; Cox, 1969; Cox and Hastenrath, 1970).

The required vertical eddy heat flux F is obtained by the integral (11). The flux is assumed to be zero at the 100-mb level near the tropopause. The mean vertical profile of F is shown in Fig. 11 in units of cal cm^{-2} day^{-1}. The vertical flux has a maximum at 700 mb, a slight minimum near 900 mb, and its largest value (389 cal cm^{-2} day^{-1}) at the sea surface.
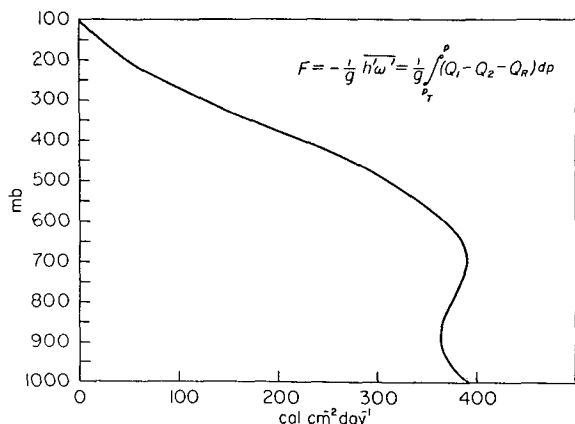

FIG. 11. The derived vertical eddy heat flux.

e. Calibration of the large-scale budgets

Although the average value of F_0 falls in the range of previous estimates of sensible plus latent heat flux by Garstang (1967) and Holland and Rasmusson (1973), we do not achieve good agreement with the direct surface observation of precipitation nor with an estimate of the evaporation using a bulk aerodynamic computation. Assuming the usual small Bowen ratio in the tropics, the integral relations (12), (13) and (14) may be approximately written

$$\frac{1}{g}\int_{p_T}^{p_0}(Q_1-Q_R)dp \approx LP_0 \quad (1086 \text{ cal cm}^{-2} \text{ day}^{-1}) \quad (12a)$$

$$\frac{1}{g}\int_{p_T}^{p_0}Q_2 dp = L(P_0-E_0) \quad (697 \text{ cal cm}^{-2} \text{ day}^{-1}) \quad (13)$$

$$F_0 \approx LE_0 \quad (389 \text{ cal cm}^{-2} \text{ day}^{-1}) \quad (14a)$$

The average numerical values from the integrations are shown in the parentheses. Thus, the heat and moisture budget computations (using the Dopplick radiation estimate) require about 1.8 cm day^{-1} of precipitation and 0.6 cm day^{-1} of evaporation.

We made an independent analysis of the observed precipitation amounts in the Marshall Islands area, which is shown in Fig. 12. The average precipitation amount in the pentagonal region is approximately 1.0 cm day^{-1}. It should be noted that the precipitation has a large horizontal gradient in the region. The southern periphery of the pentagonal region is situated on the mean ITCZ and the northern periphery is located in the relatively dry tradewind region. This is evidenced also by the analysis of the mean cloudiness.

The independent calculation of the rate of evaporation (and sensible heat flux) is a more difficult problem. We note that our cloud base conditions (Section 2d)
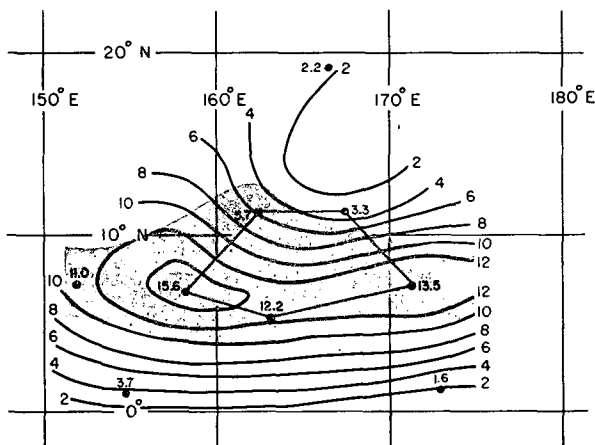

FIG. 12. Average daily precipitation (mm day^{-1}) during the period from 15 April to 22 July, 1956. The area of mean cloudiness more than 6/8 is shaded.

require a determination of the Bowen ratio. We took the rate of surface evaporation E_0 and the Bowen ratio B to be

$$E_0 = \rho C_q(q_0-q_a)V_a, \quad (77)$$

$$B = \frac{c_p(\theta_0-\theta_a)}{L(q_0-q_a)}. \quad (78)$$

In the above, ρ, C_q, q, θ and V are the density of air in the surface layer, the empirical bulk aerodynamic coefficient for latent heat flux, specific humidity, potential temperature, and the absolute air velocity. The subscripts 0 and a refer to sea surface and anemometer level, respectively.

The meteorological data of Operation Redwing have several deficiencies for the computation of (77) and (78). Only one ship near Bikini Island, the U.S.S. *Estes* (see Fig. 5), had suitable records for the bulk aerodynamic computations. However, since most of the islands are small in size, it was assumed that by using sea surface temperatures extrapolated from monthly mean charts (U.S. Department of Interior, 1968), standard surface observations taken at the island stations would also provide a rough estimate of the evaporation and the Bowen ratio over the pentagonal region. All the surface observations (eight times per day) were used.

The Bowen ratio was computed for each of the nearly 800 observations. The time-averaged Bowen ratio for the pentagonal region was 0.076. This value agrees favorably with the previous estimates made for the eastern Caribbean by Bunker (1960), Garstang (1967), and Holland and Rasmusson (1973).

A value of 1.23×10^{-3} was adopted for the 8 m bulk aerodynamic coefficient C_q, as suggested by Pond *et al.* (1971). It has an uncertainty of about 20%. The anemometer aboard the *Estes* was mounted at 14 m above the sea surface so that a correction was applied to C_q. The resulting average evaporation for the pentagonal region was 0.24 cm day^{-1}. The *Estes* data gave an evaporation rate of 0.33 cm day^{-1}.

There are a number of possible reasons for the disagreement between the large-scale budgets and the surface observations.

1) The radiational cooling rate given by Dopplick may not be adequate for this region which has a large amount of cloud cover and active cumulus convection. The actual cooling rate is likely to be much less.

2) The observed surface precipitation values are likely to be too low. In the original data tabulation, there is no clear distinction between small rain amounts and missing observations; they had to be assumed zero.

3) An examination shows that the geographical distribution of the computed evaporation is almost entirely the result of the surface wind distribution. According to the Joint Task Force Seven (1956), the observation sites of Eniwetok, Rogerik, Kwajalein, Wake

and Tarawa are excellent and entirely unobstructed. The Majuro and Kapingamarangi sites are excellent but are partially screened by palm trees. Ponape, Kusaie and Truk have island obstructions. Nearly all the stations with partial screening or island obstructions showed significantly less variance in the total wind velocity. We believe that this island effect resulted in an underestimate of the evaporation on the order of 0.1 cm day^{-1}.

4) Despite the use of a sophisticated method employed for the line integrations (Appendix), the average distance between the upper air stations was probably too large to obtain accurate estimates of the mass, heat and water vapor fluxes. This makes the estimates of Q_1 and Q_2 inaccurate.

We therefore conclude that our estimates of Q_1-Q_R and Q_2 may have errors of a factor 1.5–2.0. But in the following test computations of the cumulus ensemble properties, we do not apply any corrections on the values of Q_1, Q_2 and Q_R. Thus, there will be an internal consistency of the precipitation amount derived from the model with the initially determined heat and moisture budgets.

5. Average properties of cumulus ensembles

a. Finite-difference computational scheme

The equations mentioned in Sections 2d and 2e were applied to a 18-layer model of the cumulus ensemble. All the vertical differentiations were replaced by finite differences. The cloud base was assumed to be at 950 mb. Prior to the computation, the input data of Q_1 and Q_2 were subjected to a low-pass filter to remove diurnal variations, which smoothed out some of the noise while reducing the number of samples from 390 to 386.

In addition to the cloud base conditions (with a fixed value of the Bowen ratio of 0.076), we need a boundary condition for the liquid water equation (69), i.e., $\bar{\bar{l}}=0$ at the cloud base.

We applied Eqs. (62)–(71) to the 386 cases. The iteration converged for 366 cases. Detailed studies have not yet been made of the individual cases. In the following we show only the *time-averaged vertical distributions* of the 366 samples.

b. Cloud mass flux

Fig. 13 shows the average vertical profiles of the cloud mass flux M_c, the large-scale mean mass flux $\bar{M} = -\bar{\omega}$, and the residual mass flux in the environment, $\tilde{M}=\bar{M}-M_c$.

The most important feature seen in this diagram is that M_c exceeds $\bar{M}$ except near the tropopause; i.e., the upward mass flux in active cumulus clouds is larger than the mass flux required from the large-scale horizontal convergence. Another significant feature is
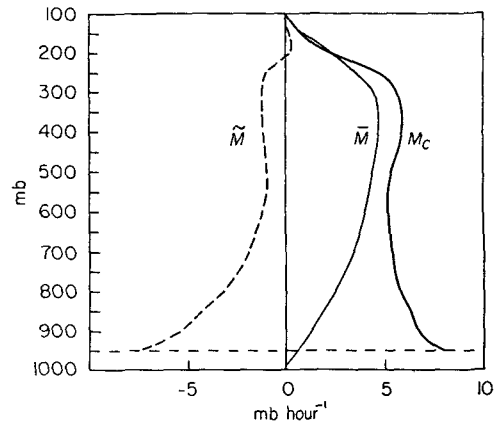

Fig. 13. The average cloud mass flux M_c (solid), large-scale mass flux $\bar{M}$ (thin solid), and residual mass flux $\tilde{M}$ (dashed).

that M_c is very large near the cloud base. This suggests that a large number of shallow cumulus clouds co-exist in the region with taller cumulonimbi. Remember that $M_c=\sum_i m_i$ (35).

As a result of the large M_c, the residual mass flux is generally downward. This sinking motion warms the environment by adiabatic compression.

c. Entrainment and detrainment

The average vertical distributions of entrainment and detrainment are shown in Fig. 14. Because of the coexistence of a variety of cloud types, entrainment ϵ and detrainment δ take place at the same height. The average entrainment is largest in the lowest layer, with a weak secondary maximum centered at about 450 mb. The entrainment goes to zero at the top of the troposphere. On the other hand, the average detrainment has two strong maxima, i.e., in the lowest layer and near the 200-mb level. The lower maximum must be the result of large number of shallow clouds that detrain immediately above the cloud base.
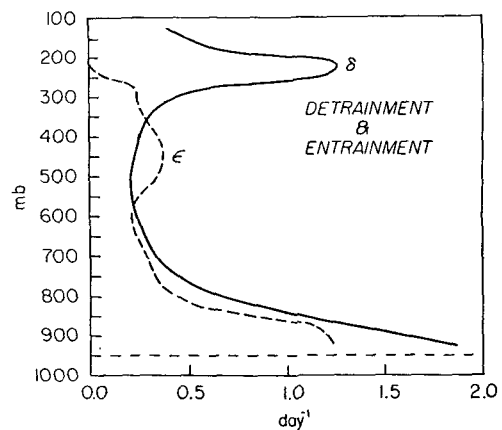

Fig. 14. The average detrainment δ (solid) and entrainment ϵ (dashed).

d. Moist static energy of clouds

The mean vertical profile of the moist static energy of the cloud ensemble, $\bar{h}_c = (\sum_i m_i h_{ci})/M_c$ [see (37)], is shown together with the average profiles of $\bar{h}$ and $\bar{h}^*$ in Fig. 15. There are several interesting features in the shape of this profile.

Near the cloud base, h_c (84.0 cal gm⁻¹) is almost equal to $\bar{h}^*$, the saturation value of static energy of the environment. Thus, the cloud air has practically zero buoyancy. This fact is consistent with the early observation of the tradewind moist layer made by Malkus (1958) and a more recent report by Simpson and Wiggert (1971).

Another noteworthy feature is that the average $\bar{\bar{h}}_c$ increases with height in the upper troposphere. Because of the definition of $\bar{\bar{h}}_c$, this indicates that we are sampling less diluted, warmer clouds in the upper troposphere. Near the tropopause $\bar{\bar{h}}_c$ has nearly the same value as at the cloud base. This tends to confirm the existence of undilute "hot towers" hypothesized by Riehl and Malkus (1958). Extending a spherical vortex model of Levine (1959), Malkus (1960) showed that large cloud elements can reach the tropopause without much dilution.

On the right-hand side of Fig. 15, the excess static energy $\bar{\bar{h}}_c - \bar{h}$ is shown. The excess reaches the maximum (3.7 cal gm⁻¹) near 650–700 mb.

e. Cloud temperature, moisture and liquid water content

In Fig. 16 the average profiles of the excess temperature $\bar{\bar{T}}_c - \bar{T}$, the excess mixing ratio $\bar{\bar{q}}_c - \bar{q}$, and the liquid water content $\bar{\bar{l}}$ of the cloud ensemble are shown.

The excess temperature of the cloud rapidly increases from -0.1C at the cloud base to 3.1C near 500 mb.
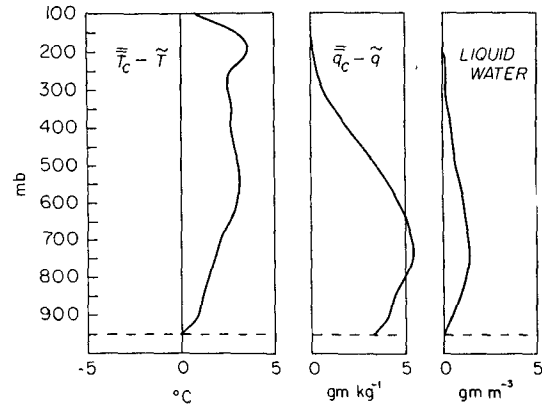
FIG. 16. The average excess temperature, excess mixing ratio, and liquid water content of the cloud ensembles.

Corresponding to the secondary maximum of the entrainment (see Fig. 14), the excess temperature decreases with height from about 500 to 250 mb, and then increases to the maximum near 200 mb. The comparison of the derived excess temperature with observations is difficult because there is very little literature on cloud temperatures excepting the classical data obtained for shallow trade cumuli in the Caribbean (roughly between 800 and 930 mb), which were reported by Malkus (1952, 1954, 1958) and Bunker (1959). According to Malkus (1958), the excess temperatures of active buoyant part of these cumuli are on the order of 2C. On the other hand, there are also active downdrafts in the clouds, which have typical temperature deficits of -1C. We feel, therefore, that the derived excess temperature is probably slightly overestimated.

The magnitude of the excess mixing ratio (the maximum value is 5.4 gm kg⁻¹ at 750 mb) also seems to be too large when compared with the previous observations (Malkus, 1954, 1958; Bunker, 1959). However, Bunker et al. (1949) reported a sounding made in a cumulus cloud, which showed an excess of 5 gm kg⁻¹ at about 1.4 km height. From a balance requirement for the vertical transport of water vapor in the tradewind cloud layer, Malkus (1962) estimated an excess mixing ratio of 5.6 gm kg⁻¹ at the same height.

The average liquid water content (gm m⁻³) of the cloud ensemble looks very reasonable, despite our crude parameterization of the precipitation process. There are a rather large number of studies on the liquid water content of maritime cumuli (Warner, 1955, 1970; Squires, 1958; Warner and Squires, 1958; Ackerman, 1959; Telford and Warner, 1962; Simpson et al., 1965; Simpson and Wiggert, 1969). Ackerman (1963) measured the liquid water content in hurricanes.

It is customary to discuss the vertical distribution of the *relative liquid water content* (the ratio of mean liquid water content sampled in clouds to its adiabatic value) as shown in Fig. 17. We note that the computed relative water contents in lower levels are much higher than the observed values in shallow cumuli reported by
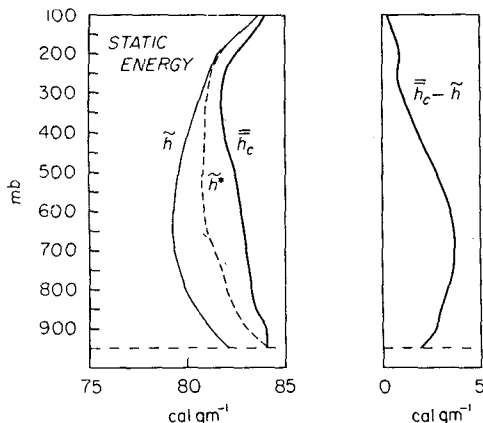

FIG. 15. Left: The average moist static energy of the cloud ensembles $\bar{h}c$ (solid), compared with the moist static energy $\bar{h}$ (thin solid) and saturation moist static energy $\bar{h}^*$ (dashed) of the environment. Right: Excess moist static energy of the cloud ensembles.

Warner (1955), Squires (1958) and Ackerman (1959). The highest altitude of observation made in hurricanes by Ackerman (1963) is 18,000 ft above the cloud base. It is interesting that the high-level portion of our computed curve seems to join with Ackerman's hurricane curve rather smoothly.

f. Condensation, precipitation and re-evaporation

It was shown in Eqs. (46) and (47) that the liquid water equation for the cloud ensemble is

$$-\bar{\delta l}+\frac{\partial M_c\bar{l}}{\partial p}+\bar{c}=K(p)\bar{l},$$

in which the rate of precipitation (the right-hand side) is very crudely parameterized. Formally, the form resembles those used by Kessler (1965, 1969) and Ogura and Takahashi (1971). However, in our model this term gives the rate of precipitation per unit mass of air (resulting from all clouds) as a function of pressure, so that a number of factors such as the cloud amount should be implicitly involved in $K(p)$. After several experiments to test the convergence of the scheme, $K(p)$ was assumed to increase nearly exponentially from 0 at the cloud base to 60.0 day^{-1} ($\sim 10^{-3}$ sec^{-1}) in the top layer. The assumption is admittedly crude and empirical. However, this crude treatment
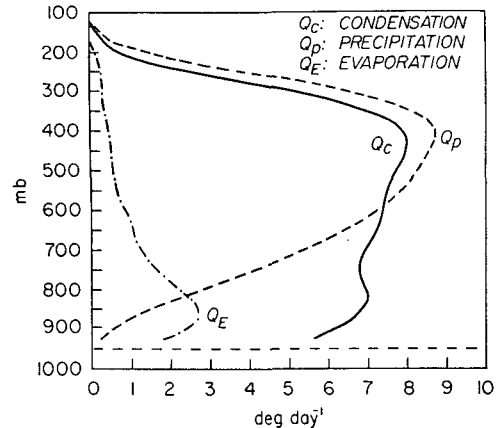
FIG. 18. The average rates of condensation Q_c (solid), precipitation Q_p (dashed) and re-evaporation Q_E (dash-dotted), in equivalent heating units.

still yields rather reasonable results for the vertical distribution of the generation of raindrops.

In Fig. 18, the vertical distributions of the mean rate of condensation, precipitation and evaporation of clouds are shown together in equivalent heating units. As required by the large-scale heat budget, the release of the latent heat associated with the precipitation is nearly 1000 cal cm^{-2} day^{-1}. In the upper troposphere the curve of precipitation is shifted upward by the vertical transport of liquid water. In the lower troposphere the rate of generation of raindrops is much smaller than the rate of condensation. Instead, a large amount of re-evaporation of clouds is taking place. The efficiency of the rain generation process (the ratio of the total precipitation to the total condensation) is about 84%.

g. Heat balance of the environment

Having obtained all the variables which characterize the cloud cluster, we can discuss the observed apparent heat source in terms of the interaction between the clouds and the environment. As shown in (49) the heat source is expressed as

$$Q_1-Q_R=-M_c\frac{\partial\bar{s}}{\partial p}-L\bar{e},$$

i.e., the sum of the adiabatic heating due to the compensating downward motion in the environment and the cooling due to evaporation of cloud droplets. These are also discussed by Gray (1971, 1972). By assumption (38), there is no detrainment of sensible heat from the clouds to the environment, except in the uppermost layer. These three features are shown in Fig. 19.

The clouds act as a heating agent primarily *through their induction of the compensating descent* $(-M_c)$. This interpretation does not mean that the actual mass flux in the environment, $\tilde{M}=\bar{M}-M_c$, must necessarily be downward. However, nearly all the computations show that $\tilde{M}$ is negative.
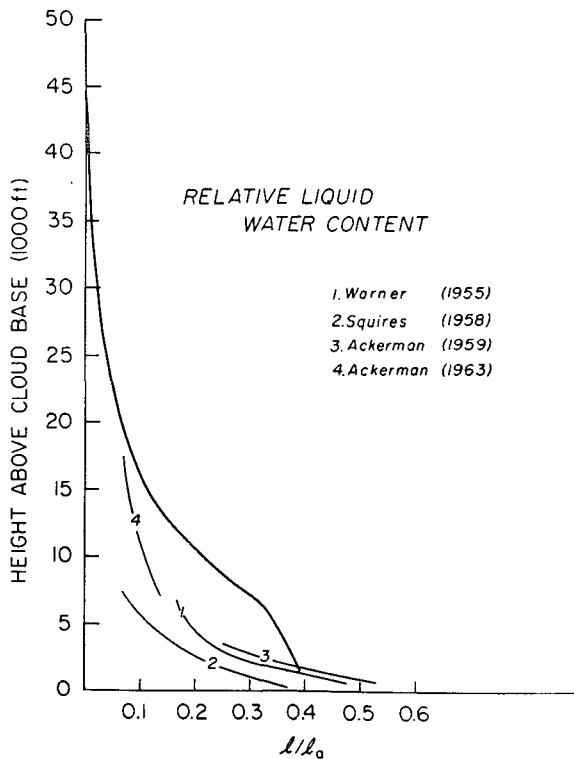

FIG. 17. The average relative liquid water content $(\bar{l}/l_a)$ of the cloud ensembles (computed value, thick line), observed results (thin lines).

RELATIVE LIQUID
WATER CONTENT

1. Warner   (1955)
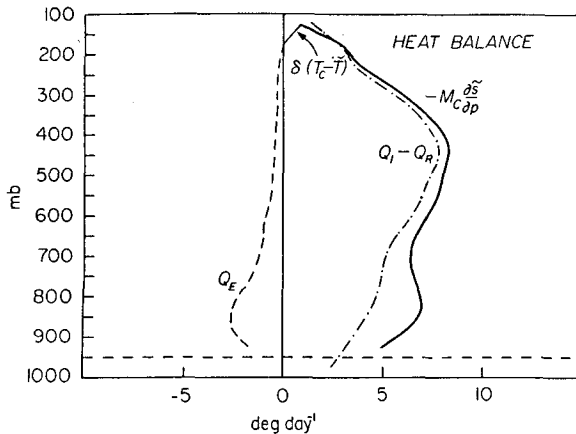2. Squires   (1958)
3. Ackerman (1959)
4. Ackerman (1963)

FIG. 19. The observed heat source Q_1-Q_R (dash-dotted), adiabatic heating by the compensating downward mass flux $-M_c(\partial \bar{s}/\partial p)$ (solid), evaporative cooling $-Q_E=-Le$ (dashed), and detrainment of heat $\delta(\bar{T}_c-\tilde{T})$ (thin solid).

The second important contribution to the apparent heat source is the cooling due to re-evaporation of the detrained cloud droplets. This effect is pronounced in the lower troposphere.

h. Moisture balance of the environment

The average moisture balance of the environment is shown in Fig. 20, in units of gm kg^{-1} day^{-1}, and also in equivalent heating units. We note from (50) that

$$-Q_2/L \equiv \frac{\partial \bar{q}}{\partial t}+\overline{\nabla\cdot(q\mathbf{V})}+\frac{\partial(\bar{q}\bar{\omega})}{\partial p}$$

$$=-M_c\frac{\partial \tilde{q}}{\partial p}+\delta(\tilde{q}^*-\tilde{q}+\bar{\bar{l}}).$$

The *apparent moisture sink* (Q_2) is primarily due to the induced downward motion $(-M_c)$. This factor alone would dry out the environmental air. It is the detrainment of water vapor and of liquid water from the clouds which makes up the balance needed to maintain the moisture of the environmental air.

This would imply that the shallower, non-precipitating cumulus clouds are needed to help the growth of the deep, precipitating cumulus towers by supplying the moisture. It is known from photographic observations that large-sized clouds are surrounded by great numbers of small cloudlets (Malkus, 1958).

6. Conclusions and future work

We have shown that by combining the large-scale heat and moisture budgets and an entrainment-detrainment model of a cumulus cloud ensemble, a large amount of information can be obtained about the bulk properties of tropical cloud clusters.

Because of the uncertainty inherent in the data used for our illustrative example, the derived quantities,

such as the cloud mass flux, the excess cloud temperature, etc., in this particular case, may be in error by a factor of 1.5–2.0.

The most important conclusion of this study is that *the cloud mass flux exceeds the mean vertical mass flux required by the large-scale convergence, thus causing a compensating sinking motion between active clouds. The large-scale heating of the environmental air is primarily due to its adiabatic compression in the compensating downward motion. The cooling due to re-evaporation of liquid water detrained from the clouds is also an important factor in the heat balance of the environment. Counteracting the drying due to the environmental sinking motion are the large amounts of water vapor and liquid water which are detrained from the clouds, especially from the shallow clouds in the lower troposphere.* Thus, the shallower, non-precipitating cumulus clouds, by their vertical transfer of water vapor, support the growth of the deep, precipitating cumulus towers. Some of the above conclusions were also reached by Gray (1972) from an independent approach.

In this study, we discussed only the time-averaged vertical distributions of the cloud cluster parameters. An examination of the day-to-day changes of these parameters, together with the changes of the large-scale atmospheric state variables, may yield additional information about the interaction between cumulus convection and the large-scale tropical motions.

In this section, we wish to point out several defects in the reported study, which are subject to future improvements.

(i) The chosen pentagonal region may be too large to be viewed as a portion of large-scale motion systems. As evidenced by the analyses of rainfall and evaporation amounts, the region contains substantial horizontal variations of the large-scale parameters. In particular, the possible horizontal gradient of the large-scale vertical motion causes an ambiguity in the interpretation of $\overline{h'\omega'}$. We plan to sub-divide the region to reveal the regional differences of the cumulus cluster properties between the ITCZ and the relatively dry tradewind regime.

(ii) There is some evidence which suggests the existence of short-lived mesoscale organization of cumulus convection (e.g., Zipser, 1969). If this is true in general, further modification of the formulation will be needed.

(iii) The weakest part of the present study is the crude parameterization of precipitation processes. Unless the area ratio σ is specified we have no way to obtain the vertical velocity in the cumulus clouds and hence the detailed cloud physical processes which were bypassed in this study.

Finally, we stress the need for better, carefully designed observational programs. To apply our method of computation, better data sets are needed to obtain accurate estimates of the heat and moisture budgets
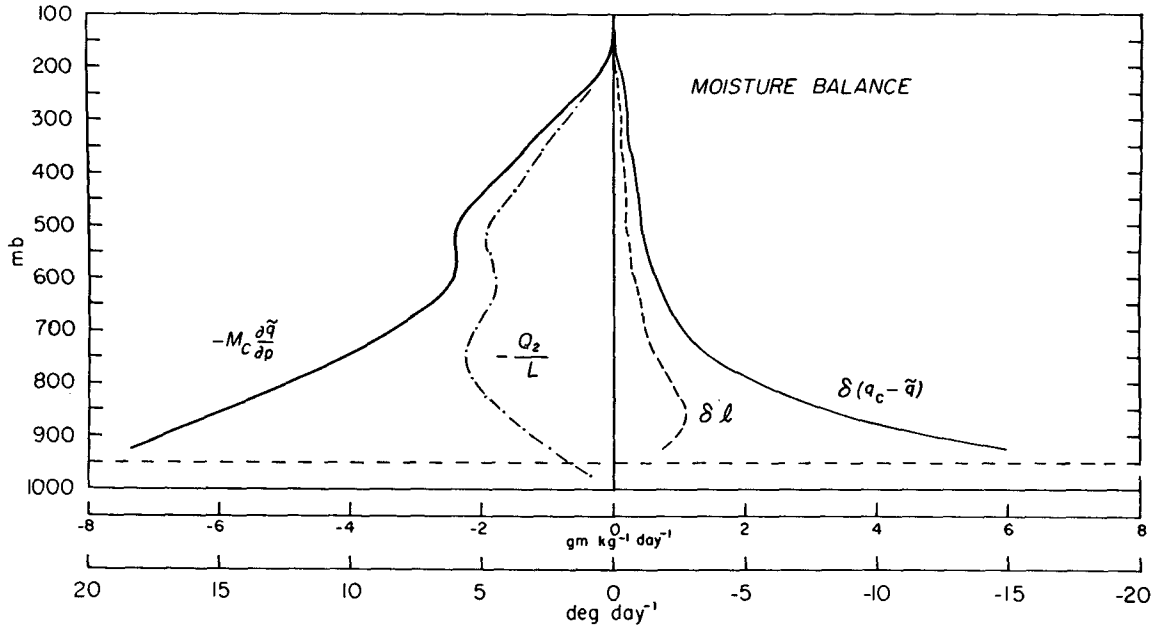
FIG. 20. The observed moisture source $-Q_2/L$ (dash-dotted), drying due to compensating sinking motion $-M_c(\partial \tilde{q}/\partial p)$ (solid), detrainment of water vapor $\delta(\bar{q}_c - \bar{q})$ (thin solid), and detrainment of liquid water $\delta \bar{l}$ (dashed), in units of gm kg^{-1} day^{-1} and in equivalent heating units ($^\circ$C day^{-1}).

over, say, a 300-km square area. This must be accompanied by equally accurate measurements of radiational cooling. The measurements of precipitation and evaporation also needed to be improved, and the internal structure of the cloud clusters should be directly sampled by aircraft. We hope that the currently planned GATE experiment will yield such a data set.

APPENDIX

Objective Analysis of Large-Scale Field Variables

Stations Eniwetok, Ponape, Kusaie, Majuro and Rongerik form a pentagon (Fig. 5). Let x_i, y_i ($i=1, 2, \ldots, 5$) be the longitudinal and latitudinal distances relative to the center of gravity of the pentagon.

Let u_i ($i=1, \ldots, 5$) be an arbitrary scalar field variable (zonal wind component, for example) observed at the stations.

We assume that

$$u_i = Ax_i^2 + Bx_iy_i + Cy_i^2 + Dx_i + Ey_i + F. \quad (A1)$$

Because we have six coefficients to be determined from five observed values of u_i, we impose the additional constraint that the curvature of the quadratic surface should be minimized as in the case of skilled hand analysis. Thus, we minimize

$$\left(2\frac{\partial^2 u}{\partial x \partial y}\right)^2 + \left(\frac{\partial^2 u}{\partial x^2} - \frac{\partial^2 u}{\partial y^2}\right)^2 = 4[B^2 + (A-C)^2]. \quad (A2)$$

Eq. (A1) may then be written

$$Ax_i^2 + Bx_iy_i + Cy_i^2 + Dx_i + Ey_i = u_i - F. \quad (A3)$$

The imposed condition is expressed as

$$B\frac{\partial B}{\partial F} + (A-C)\left(\frac{\partial A}{\partial F} - \frac{\partial C}{\partial F}\right) = 0. \quad (A4)$$

Solving

$$\frac{\partial A}{\partial F}x_i^2 + \frac{\partial B}{\partial F}x_iy_i + \frac{\partial C}{\partial F}y_i^2 + \frac{\partial D}{\partial F}x_i + \frac{\partial E}{\partial F}y_i = -1, \quad (A5)$$

we obtain

$$\partial A/\partial F, \quad \partial B/\partial F \quad \text{and} \quad \partial C/\partial F.$$

Because

$$B = \frac{(A-C)}{\dfrac{\partial B}{\partial F}}\left(\frac{\partial C}{\partial F} - \frac{\partial A}{\partial F}\right) = b(A-C), \qquad (A6)$$

(A1) reduces to

$$A\,(x_i^2 + bx_iy_i) + C\,(y_i^2 - bx_iy_i) + Dx_i + Ey_i + F = u_i. \qquad (A7)$$

Since (A7) has only five unknown coefficients, it is solvable from five observed values of u_i.

All the field variables reported in Section 4 were analyzed by this method.

Line integrals such as $\oint u\,dx$, $\oint u\,dy$, and the areal average $\bar{u} = (\text{area}^{-1})\int\int u\,dx\,dy$ were exactly obtained by using the analytical expression (A7).

The results of the mass flux computation ($\oint u\,dy - \oint v\,dx$) using the present method were compared with those obtained with the conventional linear interpolation method. For the time-averaged flux, both methods give almost identical results, but the present method gives smoother results for the daily values.

REFERENCES

Ackerman, B., 1959: The variability of the water contents of tropical cumuli. *J. Meteor.*, **16**, 191–198.

——, 1963: Some observations of water contents in hurricanes. *J. Atmos. Sci.*, **20**, 288–298.

Arakawa, A., 1969: Parameterization of cumulus convection. *Proc. WMO/IUGG Symp. Numerical Prediction*, Tokyo, IV 8, 1–6.

——, 1971: A parameterization of cumulus convection and its application to numerical simulation of the tropical general circulation. Paper presented at the 7th Tech. Conf. Hurricanes and Tropical Meteorology, Barbados, Amer. Meteor. Soc.

——, 1972: Parameterization of cumulus convection. Design of the UCLA General Circulation Model. Numerical Simulation of Weather and Climate, Tech. Rept. No. 7, Dept. of Meteorology, University of California, Los Angeles.

——, and W. H. Schubert, 1973: Interaction of a cumulus cloud ensemble with the large-scale environment. (To be published.)

Bates, J. R., 1972: Tropical disturbances and the general circulation. *Quart. J. Roy. Meteor. Soc.*, **98**, 1–16.

Bunker, A. F., 1959: Cloud and environment vertical velocities, temperatures, humidities, and water contents associated with a shear zone in the trade winds. Ref. No. 59-42, Tech. Rept. 44, Woods Hole Oceanographic Institution.

——, 1960: Heat and water-vapor fluxes in air flowing southward over the western north Atlantic ocean. *J. Meteor.*, **17**, 52–63.

——, B. Haurwitz, J. S. Malkus and H. Stommel, 1949: Vertical distribution of temperature and humidity over the Caribbean Sea. *Papers Phys. Oceanogr. Meteor.*, **11**, No. 1, 82 pp.

Chang, C.-P., 1970: Westward-propagating cloud patterns in the tropical Pacific as seen from time-composite satellite photographs. *J. Atmos. Sci.*, **27**, 133–138.

Charney, J. G., and A. Eliassen, 1964: On the growth of the hurricane depression. *J. Atmos. Sci.*, **21**, 68–75.

Cox, S. K., 1969: Observational evidence of anomalous infrared cooling in a clear tropical atmosphere. *J. Atmos. Sci.*, **26**, 1347–1349.

——, and S. L. Hastenrath, 1970: Radiation measurements over the equatorial central Pacific. *Mon. Wea. Rev.*, **98**, 823–832.

Dopplick, T. G., 1970: Global radiative heating of the earth's

atmosphere. Rept. No. 24, Planetary Circulation Project, Dept. of Meteorology, M. I. T., 128 pp.

Garstang, M., 1967: Sensible and latent heat exchanges in low-latitude synoptic-scale systems. *Tellus*, **19**, 492–508.

Gray, W. M., 1971: The magnitude and fundamental role of the up-moist and down-dry vertical circulation of the troposphere. Paper presented at the 7th Tech. Conf. Hurricanes and Tropical Meteorology, Barbados, Amer Meteor. Soc.

——, 1972: Cumulus convection and large-scale circulations, Part III. Broad scale and meso scale considerations. Atmos. Sci. Paper No. 190, Colorado State University, 80 pp.

Hastenrath, S., 1971: On meridional circulation and heat budget of the troposphere over the equatorial Central Pacific. *Tellus*, **23**, 60–73.

——, 1972: Daily wind, pressure and temperature variation up to 30 km over the tropical western Pacific. *Quart. J. Roy. Meteor. Soc.*, **98**, 48–59.

Hayashi, Y., 1970: A theory of large-scale equatorial waves generated by condensation heat and accelerating the zonal wind. *J. Meteor. Soc. Japan*, **48**, 140–160.

Holland, J. Z., and E. M. Rasmusson, 1973: Measurements of the atmospheric mass, energy, and momentum budgets over a 500 km square of tropical ocean. *Mon. Wea. Rev.*, **101**, 44–55.

Holton, J. R., 1971: A diagnostic model for equatorial wave disturbances: The role of vertical shear of the mean zonal wind. *J. Atmos. Sci.*, **28**, 55–64.

——, J. M. Wallace and J. A. Young, 1971: On boundary layer dynamics and the ITCZ. *J. Atmos. Sci.*, **28**, 275–280.

Janota, P., 1971: An empirical study of the planetary boundary layer in the vicinity of the intertropical convergence zone. Ph.D. thesis, Dept. of Meteorology, M. I. T., 278 pp.

Joint Organizing Committee, GARP, 1970: Report on the first session of the JOC Study Group on Tropical Disturbances, 1968, Appendix 1. *GARP Publ. Ser.*, No. 4.

Joint Task Force Seven, 1956: *Meteorological Report on Operation Redwing*, Part 1, Vols. 1–12.

Kessler, E., III, 1965: Microphysical parameters in relation to tropical cloud and precipitation distributions and their modification. *Geofis. Intern.*, **5**, 79–88.

——, 1969: On the distribution and continuity of water substance in atmospheric circulation. *Meteor. Monogr.*, **10**, No. 32, 84 pp.

Levin, J., 1959: Spherical vortex theory of bubble-like motion in cumulus clouds. *J. Meteor.*, **16**, 653–662.

Malkus, J. S., 1952: Recent advances in the study of convective clouds and their interaction with the environment. *Tellus*, **4**, 71–87.

——, 1954: Some results of a trade-cumulus cloud investigation. *J. Meteor.*, **11**, 220–237.

——, 1958: On the structure of the trade wind moist layer. *Papers Phys. Oceanogr. Meteor.*, **13**, No. 2.

——, 1960: Recent developments in studies of penetrative convection and an application to hurricane cumulonimbus towers. *Cumulus Dynamics*, C. E. Anderson, Ed., New York, Pergamon Press, 65–84.

——, 1962: Large-scale interactions. *The Sea*, Vol. 1, M. N. Hill, Ed., New York, Interscience, 88–294.

——, and H. Riehl, 1964: *Cloud Structure and Distributions over the Tropical Pacific Ocean*. Los Angeles, University of California Press, 229 pp.

Manabe, S., and J. Smagorinsky, 1967: Simulated climatology of a general circulation model with a hydrologic cycle II. Analysis of the tropical atmosphere. *Mon. Wea. Rev.*, **95**, 155–169.

——, J. L. Holloway, Jr., and H. M. Stone, 1970: Tropical circulation in a time-integration of a global model of the atmosphere. *J. Atmos. Sci.*, **27**, 580–613.

Mastenbrook, H. J., 1965: The vertical distribution of water vapor over Kwajalein Atoll, Marshall Islands. Rept. 6367, U. S. Naval Research Laboratory.

——, 1968: Water vapor distribution in the stratosphere and high troposphere. *J. Atmos. Sci.*, **25**, 299–311.

Murakami, M., 1971: On the disturbances appearing in precipitation near the ITC Zone in the tropical Pacific. *J. Meteor. Soc. Japan*, **49**, 184–189.

- – , 1972: Intermediate-scale disturbances appearing in the ITC Zone in the tropical western Pacific. *J. Meteor. Soc. Japan*, **50**, 454–464.

Murakami, T., 1972: Balance model in a conditionally unstable tropical atmosphere. *J. Atmos. Sci.*, **29**, 463–487.

Nitta, T., 1970: A study of generation and conversion of eddy available potential energy in the tropics. *J. Meteor. Soc. Japan*, **48**, 524–528.

——, 1972a: Energy budget of wave disturbances over the Marshall Islands during the years of 1956 and 1958. *J. Meteor. Soc. Japan*, **50**, 71–84.

——, 1972b: Structure of wave disturbances over the Marshall Islands during the years of 1956 and 1958. *J. Meteor. Soc. Japan*, **50**, 85–103.

Ogura, Y., 1973: Cumulus modeling and parameterization. (Submitted to *Rev. Geophys. Space Phys.*)

- –, and T. Takahashi, 1971: Numerical simulation of the life cycle of a thunderstorm cell. *Mon. Wea. Rev.*, **99**, 895–911.

Ooyama, K., 1964: A dynamical model for the study of tropical cyclone development. *Geofis. Intern.*, **4**, 187–198.

——, 1969a: Numerical simulation of the life cycle of tropical cyclones. *J. Atmos. Sci.*, **26**, 3–40.

- —, 1969b: Effects of parameterized cumulus convection on stability of wave disturbances in the tropical easterlies. Paper presented at the 6th Tech. Conf. Hurricanes, Miami, Amer. Meteor. Soc.

——, 1971: A theory on parameterization of cumulus convection. *J. Meteor. Soc. Japan*, **49**, Special Issue, 744–756.

Palmer, C. E., 1952: Tropical meteorology. *Quart. J. Roy. Meteor. Soc.*, **78**, 126–163.

Pond, S., G. T. Phelps, J. E. Paquin, G. McBean and R. W. Stewart, 1971: Measurements of the turbulent fluxes of momentum, moisture and sensible heat over the ocean. *J. Atmos. Sci.*, **28**, 901–917.

Reed, R. J., and E. E. Recker, 1971: Structure and properties of synoptic-scale wave disturbances in the equatorial western Pacific. *J. Atmos. Sci.*, **28**, 1117–1133.

Riehl, H., 1945: Waves in the easterlies and the polar front in the tropics. Misc. Rept., No. 17, Dept. of Meteorology, The University of Chicago.

——, 1948: On the formation of west Atlantic hurricanes. Misc. Rept. No. 24, Dept. of Meteorology, The University of Chicago, 1–64.

——, 1954: *Tropical Meteorology.* New York, McGraw-Hill, 392 pp.

——, 1962: Radiation measurements over the Caribbean during the autumn of 1960. *J. Geophys. Res.*, **67**, 3935–3942.

——, and J. S. Malkus, 1958: On the heat balance in the equatorial trough zone. *Geophysica*, **6**, 503–538.

- - –, and ——, 1961: Some aspects of hurricane Daisy, 1958. *Tellus*, **13**, 181–213.

Rosenthal, S. L., 1960: Some estimates of the power spectra of large-scale disturbances in low latitudes. *J. Meteor.*, **17**, 259–263.

Simpson, J., 1971: On cumulus entrainment and one-dimensional models. *J. Atmos. Sci.*, **28**, 449–455.

——, and V. Wiggert, 1969: Models of precipitating cumulus towers. *Mon. Wea. Rev.*, **97**, 471–489.

——, and ——, 1971: 1968 Florida cumulus seeding experiment: Numerical model results. *Mon. Wea. Rev.*, **99**, 87–118.

——, R. H. Simpson, D. A. Andrews and M. A. Eaton, 1965: Experimental cumulus dynamics. *Rev. Geophys.*, **3**, 387–431.

Squires, P., 1958: The spatial variation of liquid water and droplet concentration in cumuli. *Tellus*, **10**, 372–380.

Telford, J. W., and J. Warner, 1962: On the measurement from an aircraft of buoyancy and vertical air velocity in cloud. *J. Atmos. Sci.*, **19**, 415–423.

U. S. Department of the Interior, Bureau of Commercial Fisheries, 1968: *Mean Charts of Sea Surface Temperature in the North Pacific Ocean, 1949–1962.* Circ. 258, Washington, D. C.

Wada, M., 1969: Concerning the mechanism of the decaying of typhoon. *J. Meteor. Soc. Japan*, **47**, 335–351.

Wallace, J. M., 1971: Spectral studies of tropospheric wave disturbances in the tropical western Pacific. *Rev. Geophys. Space Phys.*, **9**, 557–612.

Warner, J., 1955: The water content of cumuliform cloud. *Tellus*, **7**, 449–457.

——, 1970: On steady-state one-dimensional models of cumulus convection. *J. Atmos. Sci.*, **27**, 1035–1040.

——, and P. Squires, 1958: Liquid water content and the adiabatic model of cumulus development. *Tellus*, **10**, 390–394.

Weinstein, A. I., 1970: A numerical model of cumulus dynamics and microphysics. *J. Atmos. Sci.*, **27**, 246–255.

Williams, K. T., 1970: A statistical analysis of satellite-observed trade wind cloud clusters in the western North Pacific. Atmos. Sci. Paper No. 161, Colorado State University, Fort Collins, 80 pp.

Yamasaki, M., 1969: Large-scale disturbances in a conditionally unstable atmosphere in low latitudes. *Papers Meteor. Geophys.*, **20**, 289–336.

——, 1971: Frictional convergence in Rossby waves in low latitudes. *J. Meteor. Soc. Japan*, **49**, Special Issue, 691–698.

Yanai, M., 1961a: A detailed analysis of typhoon formation. *J. Meteor. Soc. Japan*, **39**, 187–214.

——, 1961b: Dynamical aspects of typhoon formation. *J. Meteor. Soc. Japan*, **39**, 283–309.

——, 1963: A preliminary survey of large-scale disturbances over the tropical Pacific region. *Geofis. Intern.*, **3**, 73–84.

——, 1964: Formation of tropical cyclones. *Rev. Geophys.*, **2**, 367–414.

——, 1971a: A review of recent studies of tropical meteorology relevant to the planning of GATE. *Experimental Design Proposal by the Interim Scientific and Management Group (ISMG)*, Vol. 2, Annex I.

——, 1971b: The mass, heat and moisture budgets and the convective heating within tropical cloud clusters. Paper presented at the 7th Tech. Conf. Hurricanes and Tropical Meteorology, Barbados, Amer. Meteor. Soc.

Zipser, E. J., 1969: The role of organized unsaturated convective downdraft in the structure and rapid decay of an equatorial disturbance. *J. Appl. Meteor.*, **8**, 799–814.